Kovove Mater. 49 2011 163–177
DOI: 10.4149/km_2011_3_163

Properties and processing of magnesium-tin-calcium alloys

N. Hort[1], Y. D. Huang[1]*, T. Abu Leil[1], K. P. Rao[2], K. U. Kainer[1]

[1] *MagIC – Magnesium Innovation Centre, Helmholtz-Zentrum Geesthacht Centre for Materials and Coastal Research, Max-Planck-Str. 1, D-21502 Geesthacht, Germany*
[2] *City University Hong Kong, 83 Tat Chee Avenue, Kowloon, Hong Kong*

Received 3 December 2010, received in revised form 11 March 2011, accepted 14 March 2011

Abstract

The development of new creep resistant magnesium alloys has become a major issue in recent years and therefore further alloy development is necessary. Newly developed alloys are based on the binary system Mg-Sn. Sn as major alloying element was chosen due to its high solid solubility over a wide temperature range and due to the possible formation of Mg_2Sn intermetallic precipitates with a high melting temperature of about 770 °C. These characteristics suggest that a fairly large volume fraction of thermally stable Mg_2Sn particles can be formed during solidification. This makes it possible that the Mg-Sn alloys can be developed as creep resistant magnesium alloys and/or wrought magnesium alloys. Previous investigations indicate that the Mg-Sn alloys have a comparable or even better creep properties than AE42 alloy. This paper presents an overview about recent works on the developments of Mg-Sn alloys performed in MagIC, Helmholtz-Zentrum Geesthacht, which includes: microstructural characterization, creep deformation and hot deformation, and corrosion behaviour. Very positive results have been obtained and show Mg-Sn-Ca alloy systems can be developed for power train and hand tool applications.

K e y w o r d s: magnesium alloy, Mg-Sn, microstructure, creep, corrosion

1. Introduction

Reducing green house gas emissions and fuel consumption saves your money and protects the environment at the same time. In the past fifteen years magnesium alloys have been mainly of interest for automotive industries [1, 2]. The major target was and still is the reduction of weight without limiting the comfort and safety issues. Moreover, legislative requirements force the automotive industries in Europe to lower the CO_2 emissions below 140 g km^{-1} at the end of 2008 and 120 g km^{-1} at the end of 2012 as well as to ensure that 85 % of new produced cars have to be recycled. These targets can be reached by an increasing use of magnesium alloys to replace materials with higher density like aluminium alloys or even steels. Besides the competition with other metallic materials magnesium is also in competition with polymer materials. But in difference to most polymers magnesium offers higher stiffness and strength as well as typical properties of a metal like good heat and electrical conductivity and the possibility of shielding of electromagnetic waves.

In the past, cast magnesium alloy development mainly was carried out to improve corrosion behaviour as well as mechanical properties and to enhance the property profile towards the use of magnesium cast alloys at elevated temperatures beyond 150 °C [3, 4]. This led to the introduction of a number of new alloys. Examples for those new magnesium alloys are the MRI alloys used by the Volkswagen group, modified AS alloys used by Daimler and the new AJ alloys which are in use by BMW in the power train.

In the case of magnesium wrought alloys actually AZ31 is the alloy that is of most interest for the consumer as well as for researcher. New developments started based on the knowledge of the behaviour of AZ31 during deformation and in service. The aim is to improve deformability, ductility and strength of new magnesium wrought alloys. With regard to the hexagonal lattice structure of magnesium and its alloys, the deformation processes like hot extrusion,

*Corresponding author: tel.: 00494152871935; fax: 00494152871909; e-mail address: yuanding.huang@hzg.de

rolling or forging need to be designed in a way that high deformation rates can be used in low deformation temperatures. This has to be supported by alloy development to assure that at the end of the process a product stands with improved properties and a homogeneous microstructure.

In recent years the development of a new series of Mg-Sn alloys had been started at the MagIC since 2000. In these binary alloys the amount of Sn has been varied up 15 wt.% in the first. To achieve further knowledge about the influence of alloying elements these binary alloys have been modified using Al, Mn, Sr, Si, RE, and Ca. After preliminary investigations the decision was made to focus further research on ternary Mg-Sn-Ca alloys first [5–10].

The addition of Sn as well as the addition of Ca offers the possibility of both solid solution strengthening and precipitation hardening [6–8, 11–13]. With regard to the binary phase diagrams Mg-Sn-Ca are also offering the potential to change the property profile with regard to different heat treating regimes [14]. Moreover, the intermetallic compounds Mg_2Sn and Mg_2Ca are having high melting points of 770.5 ℃ and 715 ℃, respectively. Therefore they are also promising candidates to improve the creep response of those alloys. Besides these binary compounds a ternary intermetallic phase CaMgSn may appear in these alloys and contributes to further improvement of the property profile [6].

Following by MagIC, the development of Mg-Sn systems for different applications was also performed in the recent ten years by other research groups in Korea, Japan and China etc. [15–34]. Most of their investigations focus on the influences of alloying elements on the microstructure, mechanical properties and corrosion behaviour. For the binary Mg-Sn alloys, Chen et al. reported that the grain sizes of extruded and annealed alloys decreased with increasing the content of Sn [15]. Nayyeri et al. concluded that the precipitation of Mg_2Sn during ageing could enhance the creep resistance of binary Mg-Sn alloys [24]. Their results show the aged Mg-Sn binary alloys have a much better creep resistance than that of the as-cast alloys. Due to the fact that the properties of binary Mg-Sn alloys cannot meet the requirements for practical industrial applications, the optimization of alloy compositions through the additions of other alloying elements is inevitable. These alloying elements include Ca, Sr, RE (rare earths), Al, Zn and Sb. Among them, the additions of Ca, Sr or RE improves both the room temperature strength and high temperature creep resistance due to the formation of precipitates such as CaMgSn or CaMgSr. The phases CaMgSn and CaMgSr are high temperature stable. They are very effective to improve the creep resistance of Mg-Sn alloys. In Mg-Sn-Ca alloys, the size of precipitates CaMgSn can further be decreased by the additions of RE such as Y or Ce [32, 33], leading to the further improvement of mechanical properties. Like in Mg-Al alloys, Zn is also an interesting alloying element for Mg-Sn alloys. The precipitation of Mg_2Sn and $MgZn_2$ is largely enhanced in Mg-Sn alloys with the small addition of Zn (< 1 at.%) [28]. Although the alloying element Sb is unfriendly to environment, its addition refines the dendritic microstructure and modifies the morphology of Mg_2Sn precipitates [22]. It can also increase the creep resistance of Mg-Sn alloys. Certainly, the additions of alloying elements influence the corrosion resistance of Mg-Sn alloys. The previous results indicate that the addition of Sn and Sr can improve the corrosion resistance of Mg-Sn-Al-Zn alloys [26, 27].

In order to assist the alloy development, the thermodynamic calculations of Mg-Sn-Ca ternary phase diagram were performed by Kozlov et al. [18, 19]. The calculated results are quite in agreement with those obtained by experimental results [35]. Both of them demonstrate that the phase situation depends on the composition of Sn and Ca in Mg-Sn-Ca systems, especially the ratio of Sn to Ca. Main two second phases CaMgSn and Mg_2Ca are formed at the corner of Mg. Besides the Mg-Sn-Ca systems, Zhao et al. calculated the isothermal sections of Mg-Sn-Y system at high temperatures [36]. At the Mg-rich corner, a new second phase MgSnY exists.

The present paper presents an overview of the investigations on the alloy development of Mg-Sn systems done by MagIC in the last 10 years. The effects of alloying elements, especially calcium, on the microstructure, mechanical properties and corrosion behaviour are discussed.

2. Experimental procedures

2.1. Materials production

All materials have been produced in the first by permanent mould casting. The alloying elements Sn and Ca have been introduced in their pure form into the melt which was kept at 720 ℃ melt bath temperature under protective gas of Ar + 0.2 % SF_6.

Table 1 shows the compositions of some selected alloys. After addition of the alloying elements the alloys have been poured into a cylindrical permanent mould which was preheated to 200 ℃. The mould had a diameter of 100 mm and a length of 350 mm. From these castings specimens for further investigations have been manufactured.

2.2. Microstructural characterization

Microstructural investigations have been performed using light optical microscopy (LOM), scan-

Table 1. Nominal compositions of investigated Mg-Sn-Ca alloys, detected intermetallic phases and lattice parameters of primary Mg phase in the as-cast alloys

Alloy	Composition (wt.%)			Second phases	Lattice parameters	
	Sn	Ca	Mg	as-cast	a	c
Mg3Sn	3		Bal.	Mg_2Sn	3.20750	5.20871
Mg3Sn0.5Ca	3	0.5	Bal.	CaMgSn	3.20719	5.20734
Mg3Sn1Ca	3	1.0	Bal.	CaMgSn	3.20877	5.20679
Mg3Sn1.5Ca	3	1.5	Bal.	CaMgSn	3.20508	5.20918
Mg3Sn2Ca	3	2	Bal.	CaMgSn, Mg_2Ca	3.20735	5.20882
Mg5Sn	5		Bal.	Mg_2Sn	3.20670	5.20873
Mg5Sn0.5Ca	5	0.5	Bal.	CaMgSn, Mg_2Sn	3.20685	5.20606
Mg5Sn1Ca	5	1	Bal.	CaMgSn, Mg_2Sn	3.20775	5.20656
Mg5Sn1.5Ca	5	1.5	Bal.	CaMgSn	3.20689	5.20348
Mg5Sn2Ca	5	2	Bal.	CaMgSn, Mg_2Ca (very less)	3.20307	5.21120

ning electron microscopy (SEM) including energy dispersive X-ray analysis (EDX), transmission electron microscopy (TEM) and X-ray diffraction analysis (XRD). For LOM and EDX analysis standard procedures for grinding, polishing and etching were applied. Specimens for TEM were ground mechanically to about 70 μm and then thinned using electropolishing in a twin jet system using a solution of 5 % $HClO_4$ and 95 % ethanol at about –30 ℃ and a voltage of 40 V. The TEM observations were performed on a JEOL 2000 transmission electron microscope with an energy dispersive X-ray analysis (EDX) system operating at 200 kV. X-ray diffractions (XRD) were carried out using a Siemens diffractometer operating at 40 kV and 40 mA with Cu Kα radiation. Measurements were performed by step scanning 2θ from 20 to 120° with a step size of 0.02°. A count time of 3 s per step was used.

The microstructural evolution during solidification was simulated using Scheil modelling by Pandat software [37]. A comparison between the simulation and experimental results was discussed.

2.3. Mechanical behaviour

2.3.1. Creep deformation

Cylindrical specimens of 15 mm length and 6 mm diameter were used for the compressive creep tests. They were tested at a temperature of 175 ℃ subjected to a compressive stress of 80 MPa continuously for 100 h. They were performed in uniaxial compression on an ATS testing system. After heating and subsequent soaking time of 30 min the tests were started automatically. The temperature was measured with a Ni-CrNi thermocouple and maintained within the range ± 3 ℃. Besides the compression creep tests, tensile creep tests were also carried out for several alloys. They were conducted at ATS lever arm creep test systems in air under constant stress 85 MPa and constant temperature 135 ℃.

2.3.2. Hot deformation

Hot deformation trials have been performed to obtain a deeper knowledge on the deformation behaviour of the chosen alloys using the specimens with a diameter of 10 mm and a length of 15 mm. The tests were conducted using a computer-controlled servo-hydraulic machine in a 6 × 6 experimental matrix at a temperature range of 300 to 550 ℃ and strain rates ranging from 0.0003 s^{-1} to 10 s^{-1}. Graphite powder mixed with grease was used as the lubricant. All specimens were deformed up to a true strain of about 0.75 and then quenched in water. Deformation force, reduction in height, and rise in temperature of the specimen during the tests were measured during all tests.

2.4. Corrosion

Corrosion samples with 18 mm in diameter and a thickness of 4 mm were prepared in order to conduct two kinds of corrosion tests, namely, polarization and salt spray tests. For the polarization test the specimens were ground with SiC emery paper (1200 grid) on the side, where the specimen was exposed to the corrosive medium. The set up used the specimens of various alloys as working electrodes with an exposed area of 1.54 cm^2 in contact with the electrolyte, in conjunction with an Ag/AgCl reference electrode and a platinum counter electrode. The potentio-dynamic polarization measurement scan was started at –250 mV relative to the rest potential which was determined at first. The scan rate was defined as 0.2 mV s^{-1}. The corrosion rate was calculated using Tafel slope from the cathodic branch of the polarization curve.

The specimens used for the salt spray tests had the same dimensions as those used in the polarization tests but were ground on both sides. The potentio-dynamic polarization measurements were conducted at room temperature, in a 5 % NaCl solution with a pH value adjusted to 11 using NaOH. The specimens

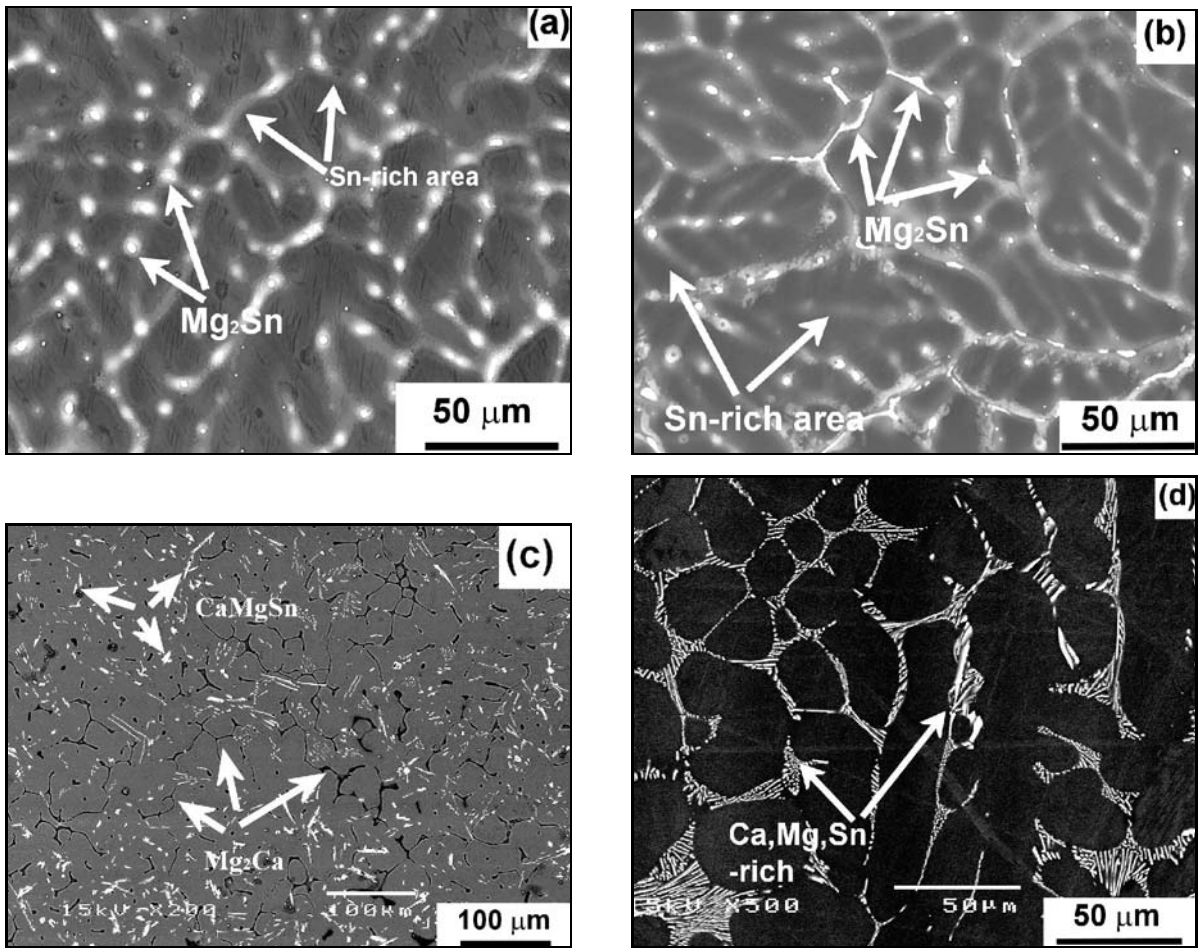

Fig. 1. SEM micrographs taken from as-cast samples of: (a) Mg-3Sn, (b) Mg-5Sn, (c) Mg-3Sn-2Ca and (d) Mg-5Sn-2Ca alloys.

were immersed in salt spray of 5 % NaCl solution of pH value 7 for 48 h. The temperature of the salt spray chamber was controlled at 35 ℃. After the test the corroded specimens were rinsed with water and cleaned in chromic acid to remove the oxides and dried subsequently. The weight loss of the specimens was used to calculate the average corrosion rate in millimetres per year.

3. Results and discussion

3.1. Microstructure

3.1.1. Microstructural evolution during solidification

In the binary Mg-Sn alloys, the dendritic boundaries are decorated with the bright globular particles and diffusive bright bands (Fig. 1a). With increasing the content of Sn from 3 % to 5 %, some particles with a lamellar shape can be observed (Fig. 1b). The compositions of the globular and lamellar phases are close to those of Mg_2Sn phase. XRD analysis also shows the existence of the phase Mg_2Sn in the binary alloys (Tables 1, 2 and Fig. 2). EDX analysis indicates that the diffusive bright bands are attributed to the enrichment of Sn at the dendritic boundaries. In these regions, the content of Sn can be up to 7 wt.% which is much higher than that in the matrix (approximately 1.2 wt.%). The volume fraction of Mg_2Sn is affected by the Sn content. The Mg_2Sn content increases with addition of the Sn content. The peaks of Mg_2Sn were detected by XRD in the as-cast Mg-5Sn alloys, but not in the as-cast condition of the Mg-3Sn alloys. Based on the Mg-Sn phase diagram, Mg_2Sn was able to precipitate below the temperature of approximately 380 ℃ in Mg-3Sn alloy and below 420 ℃ in Mg-5Sn alloy, respectively. In the as-cast Mg-5Sn alloy condition, the volume fraction of precipitated Mg_2Sn phase is high enough to be detected by XRD. The disappearance of XRD peaks, which is caused by technical limitations, cannot exclude the presence of Mg_2Sn phase in the as-cast Mg-3Sn alloy (Fig. 1a).

The grain boundary second phases show a kind of lamellar eutectic morphology with bright contrast in both the Mg-3Sn-2Ca and Mg-5Sn-2Ca al-

Table 2. Phases in the ternary Mg-Sn-Ca systems are listed to check the effect of the weight percent ratio of Sn to Ca on the formation of second phases in the Mg-Sn-Ca systems

Ratio of Sn to Ca (wt.%)	Phases		Alloys
1.0	CaMgSn, Mg_2Ca	CaMgSn, Mg_2Ca	Mg-2Sn-2.0Ca
1.5	CaMgSn, Mg_2Ca		Mg-3Sn-2.0Ca
2	CaMgSn, Mg_2Ca		Mg-3Sn-1.5Ca
2.5	CaMgSn, Mg_2Ca		Mg-5Sn-2.0Ca
3	CaMgSn	CaMgSn	Mg-3Sn-1.0Ca Mg-4.5Sn-1.5Ca Mg-6Sn-2Ca
3.3	CaMgSn		Mg-5Sn-1.5Ca
5	CaMgSn, Mg_2Sn	CaMgSn, Mg_2Sn	Mg-5Sn-1.0Ca
6	CaMgSn		Mg-3Sn-0.5Ca
10	CaMgSn, Mg_2Sn		Mg-5Sn-0.5Ca

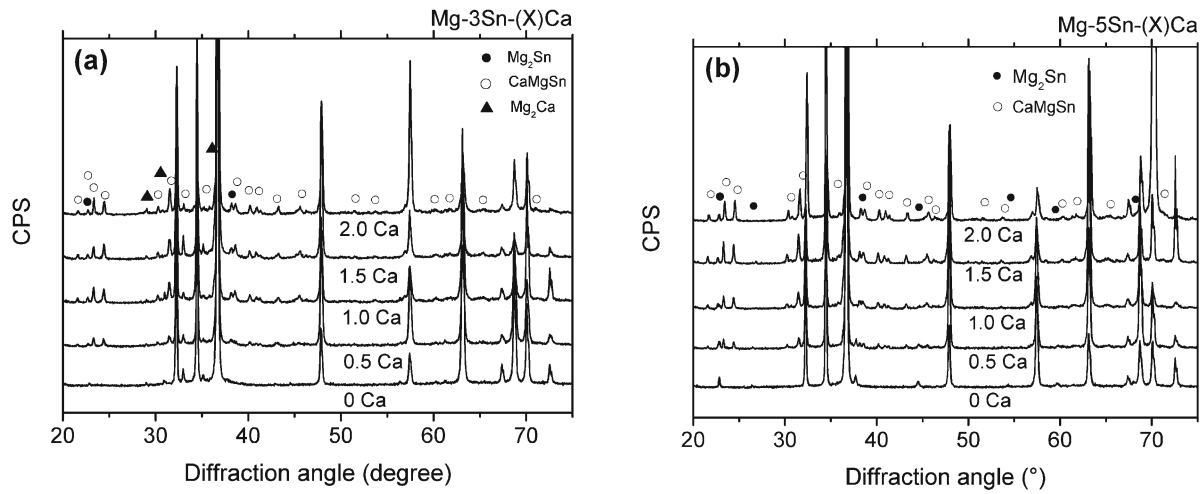

Fig. 2. XRD patterns of (a) Mg-3Sn-xCa and (b) Mg-5Sn-xCa alloys.

loys (Fig. 1c,d). No diffusive bright bands were observed in these two Ca-containing alloys. EDX analysis reveals that these lamellar precipitates are enriched with Ca, Mg and Sn. The ratio of atomic percent of Ca to Sn is about 1 : 1. XRD and TEM experiments indicate that the addition of Ca can lead to the formation of the CaMgSn phase (Figs. 2, 3, 4 and Table 2). The volume fraction of the CaMgSn phase is proportional to the content of Ca. On the other hand, the volume fraction of Mg_2Sn phase decreases in the Mg-5Sn-Ca alloys with the formation of CaMgSn phase. The addition of Ca seems to suppress the formation of Mg_2Sn phase in the Mg-Sn-Ca system (Table 1). Compared with CaMgSn particles, the precipitates Mg_2Sn are much smaller which are normally observed near the dendritic and grain boundaries (Fig. 5).

Table 2 summarizes the effect of the ratio of Sn to Ca on the second phases in Mg-Sn-Ca alloys. If the

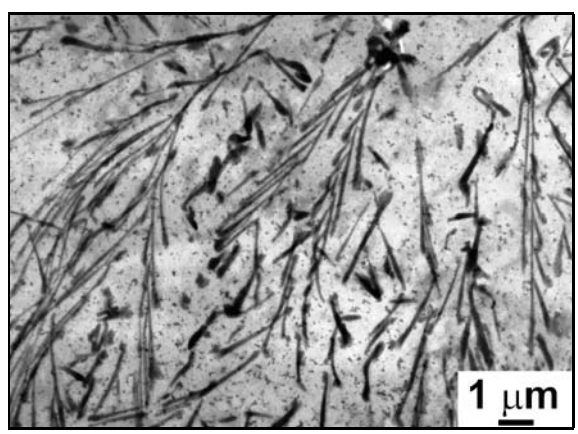

Fig. 3. Low magnification observations (TEM; bright field) of particles in the as-cast Mg-5Sn-1Ca magnesium alloy. The second phases with different shapes are observed at the dendritic or grain boundaries.

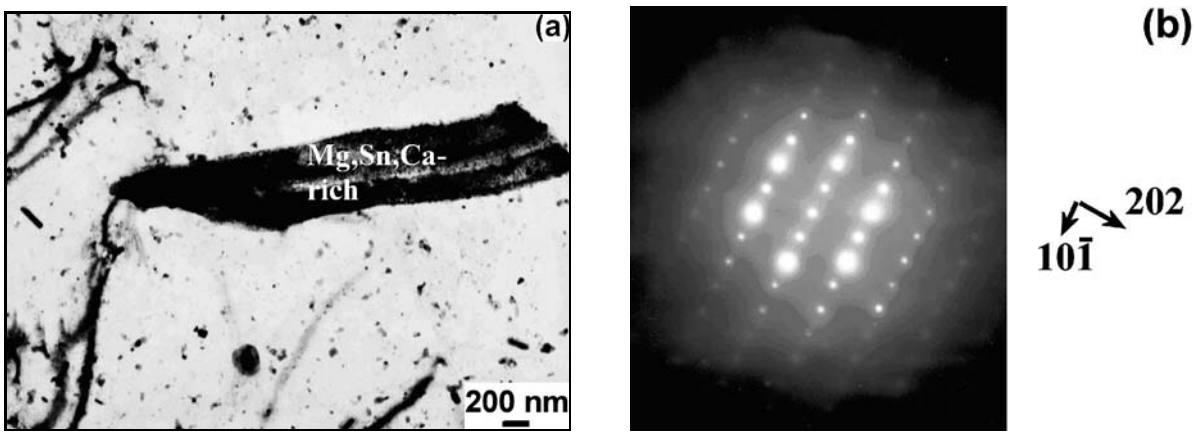

Fig. 4. Observation of the large particle in the as-cast Mg-5Sn-1Ca magnesium alloy: (a) morphology of the particle by TEM investigation and (b) diffraction pattern, the zone axis is [040]. It is identified as the phase CaMgSn.

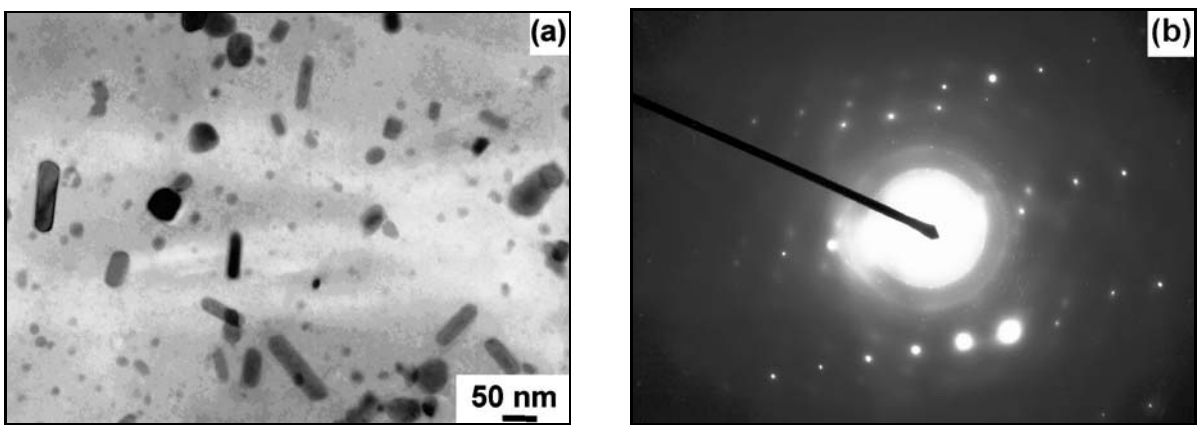

Fig. 5. Observation of the fine particles in the as-cast Mg-5Sn-1Ca magnesium alloy: (a) morphology of the particles and (b) diffraction rings from this area. The phases are identified as the Mg_2Sn phases.

ratio is less than 3, the second phases include CaMgSn and Mg_2Ca. When the ratio is in the range from 3 to 5, only CaMgSn phase is formed. If the ratio further increases to more than 5, then CaMgSn and Mg_2Sn are precipitated.

It can be clearly stated that the ternary phase CaMgSn is forming first in a precipitation sequence. As second, the α-Mg phase would form, keeping other alloying elements in a solid solution. Only in the case that there is an excess of Ca the possibility for the formation of precipitates Mg_2Ca is open, while an excess of Sn would lead to the formation of Mg_2Sn. Moreover it seems if there is no chance to precipitate Mg_2Sn as long as there is some Ca present. The presence of both Ca and Sn would lead to the formation of the ternary phase CaMgSn in any case. In fact Mg_2Sn could not be observed in any of the alloys if the ratio of Sn to Ca was less than 5. These findings are in good agreement with previous works [6, 38]. Therefore a precipitation sequence would be like the following:

$$\text{CaMgSn} \rightarrow \alpha\text{-Mg} \begin{cases} \nearrow \text{Mg}_2\text{Ca (excess of Ca)} \\ \searrow \text{Mg}_2\text{Sn (excess of Sn)} \end{cases}$$

The above analysis of experimental results is in full agreement with the thermodynamic calculation (Fig. 6).

3.1.2. Effect of heat treatment on microstructure

The volume fraction of Mg_2Sn phase is affected by the heat treatment, indicating that this phase is thermally not stable. XRD results (Fig. 7a) show that the peaks of Mg_2Sn phase can even be observed in the Mg-3Sn alloys after ageing treatment (T6). The graph presents the as-cast condition and the 500 ℃ for 6 h furnace cooled (FC), 500 ℃ for 6 h water quenched (WQ) and 500 ℃ for 6 h followed by 300 ℃ for 6 h air cooled, respectively. Due to the rapid cooling rate dur-

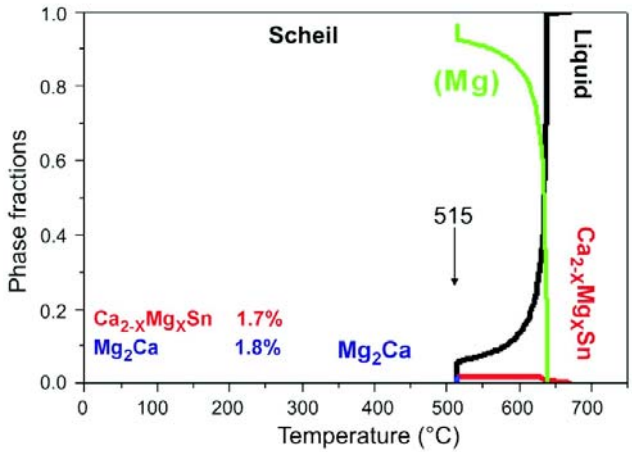

Fig. 6. Thermodynamic calculation results using Scheil's model for Mg-3Sn-2Ca alloy [18, 19].

ing casting, which suppresses the Mg_2Sn formation, less volume fraction of the Mg_2Sn phase is found in the as-cast Mg-3Sn alloy. The CaMgSn phase seems to be a very stable phase. Its volume fraction is not affected by the heat treatments. Even after the solution treatment at 500 ℃ for 6 h, the intensities of diffraction peaks keep the same level as that observed intensity in the as-cast alloy (Fig. 7b). SEM and TEM observations further confirm that this phase CaMgSn is very stable (Figs. 8 and 9). It is still clearly observed in Mg-Sn-Ca alloys after T4 solution treatment.

3.2. Creep deformation

3.2.1. Creep mechanism in binary Mg-Sn alloy

Both the tensile and compressive creep deformations demonstrate that the binary Mg-Sn alloys have a very poor creep property (Tables 3 and 4). After creep deformation, the voids are observed at the dendritic and grain boundaries where Sn is enriched (Figs. 10 and 16). With the proceeding of creep deformation,

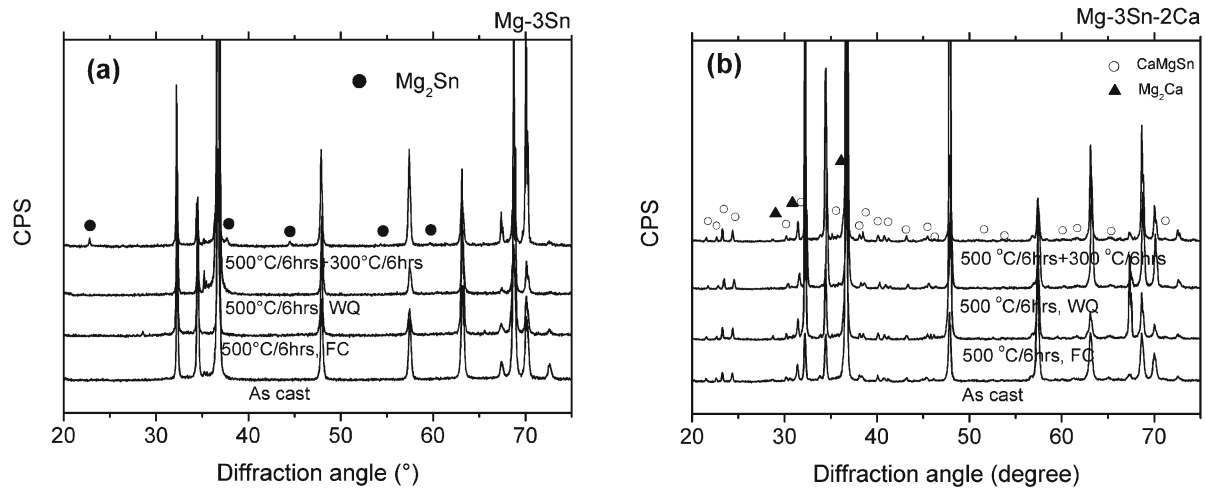

Fig. 7. XRD patterns showing the effect of heat treatments on the formation of second phases in (a) Mg-3Sn and (b) Mg-3Sn-2Ca alloys.

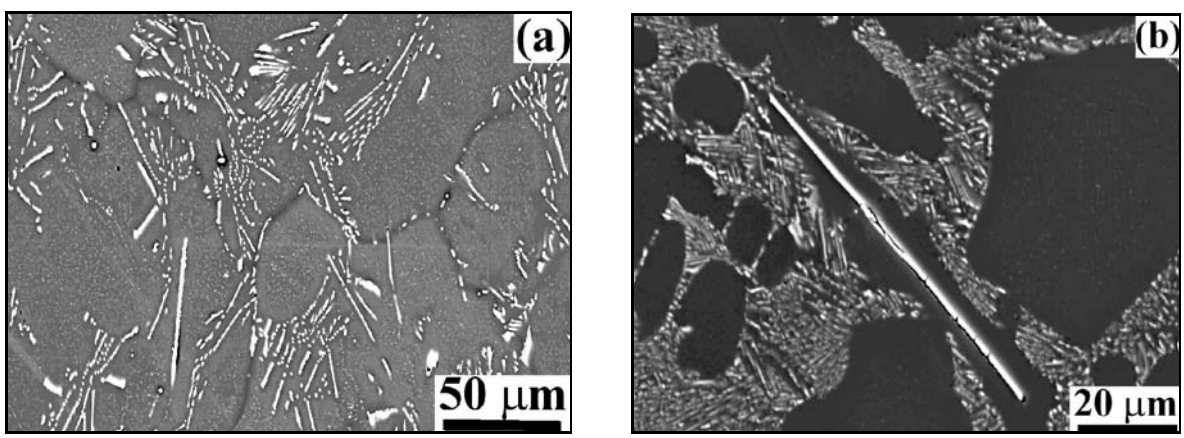

Fig. 8. SEM micrographs showing the microstructures after T4 heat treatments: (a) Mg-5Sn-1Ca and (b) Mg-5Sn-2Ca.

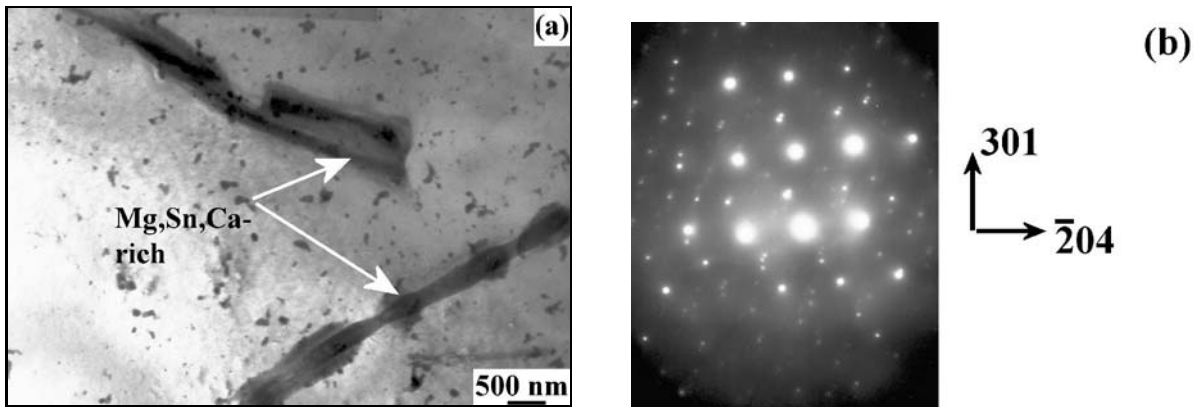

Fig. 9. Observation of CaMgSn particle in the Mg-5Sn-1Ca magnesium alloy with the T4 treatment (300 °C, 100 h): (a) TEM and (b) diffraction pattern, the zone axis is $[0, 14, 0]$.

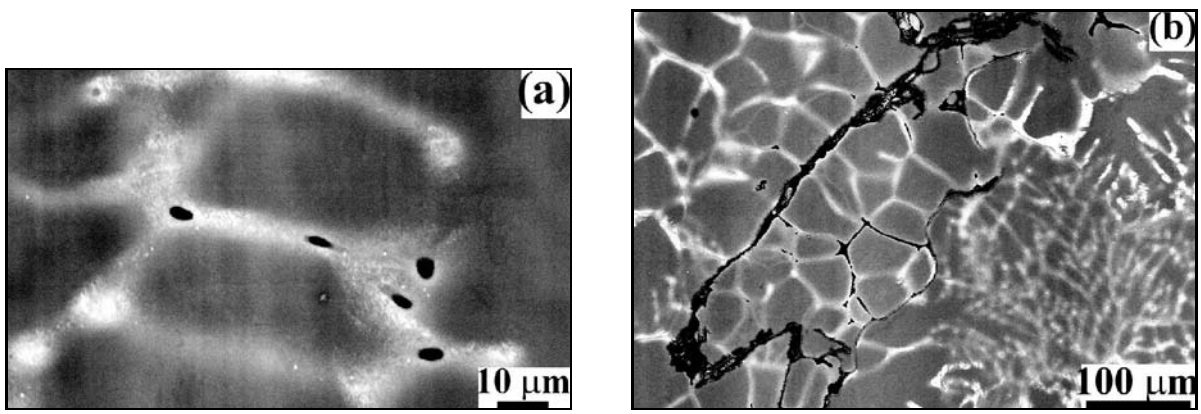

Fig. 10. Microstructures after tensile creep rupture for the as-cast Mg-3Sn binary alloy: (a) formation of voids at the triple joints of dendritic boundaries, (b) cracks propagating along the dendritic boundaries.

Table 3. Creep life of Mg-Sn alloys under the condition of 85 MPa and 135 °C (tensile creep)

Alloy No.	Alloys	Creep life (h)	Elongation (%)	Secondary creep rate (s^{-1})
1	Mg3Sn	0	0	
2	Mg3Sn2Ca	358.4	3.6	4.5×10^{-9}
3	Mg5Sn	0	0	
4	Mg5Sn2Ca	82.5	3.3	3.5×10^{-8}

Table 4. Creep rate in the time range of 140–150 h for different heat treatments (compressive creep, 135 °C and 85 MPa)

Alloy	Creep rate (s^{-1})			
	F*	FC**	T4	T6
Mg3Sn	4.34E-05	1.99E-05	1.20E-05	3.32E-06
Mg3Sn1Ca	5.14E-08	1.2E-07	2.15E-07	4.07E-07
Mg3Sn2Ca	5.61E-09	7.87E-09	1.45E-09	1.86E-08

* As-cast, ** Furnace cooling

the crack even propagates along the dendritic and grain boundaries. Based on these observed experimental phenomena, the poor creep properties of the binary Mg-Sn alloys are related to the segregation of Sn at the dendritic and grain boundaries. The segregation of Sn increases the homologous temperature in these regions, because the local solidus temperature is lower than inside the grains [39]. If the solidus shown in Mg-Sn phase diagram is approximately regarded as a line, it is then known that the solidus temperature decreases by about 6.1 °C/wt.% (26.5 °C/at.%) in Mg-Sn system. Present survey shows that the local homologous temperature is about 0.23 near the dendritic and grain boundaries (test temperature is 135 °C). In-

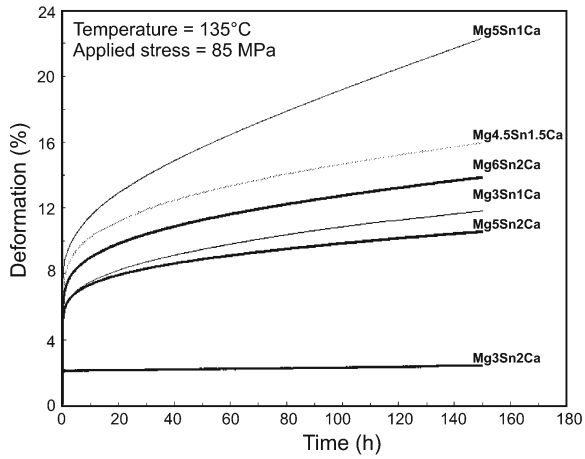

Fig. 11. Creep curves obtained for the selected Mg-Sn-Ca alloys.

side the grains, the homologous temperature decreases to about 0.21. Consequently, owing to the heavy Sn segregation in the as-cast sample, the creep deformation preferentially starts at the dendritic and grain boundaries. On the other hand, in the binary alloys, the amount of the particles Mg_2Sn decreases inside the grains because of the segregation of Sn, which weakens their pinning effects on the movement of dislocations. The creep deformation then partially proceeds by dislocation recovery.

3.2.2. Effect of Ca

After the addition of Ca to the binary Mg-Sn alloys, the creep resistance improves (Tables 3, 4 and Fig. 11). With the increment in Ca content, the creep rate decreases. For example, when the Ca content increases from 1.0 wt.% to 2.0 wt.% in Mg-3Sn-Ca systems, the creep rate decreases from $5.1 \times 10^{-8}\,s^{-1}$ to $5.6 \times 10^{-9}\,s^{-1}$.

After creep deformation, the voids and cracks are still observed at the dendritic and grain boundaries in both the Mg-3Sn-2Ca and Mg-5Sn-2Ca alloys (Fig. 12). Compared with the binary alloys (Fig. 10), the amount of voids and cracks largely decreases in these two Ca-containing alloys. It is interesting to note that the propagation of cracks normally stops in front of the particles Mg_2Ca or CaMgSn, indicating that the existence of these two phases is very effective to hinder the sliding of grain boundary. As mentioned above, CaMgSn is a thermal stable phase. In addition, the addition of Ca alleviates the segregation of Sn due to the depletion of Sn by the formation of the Ca-containing intermetallics CaMgSn. All these factors are beneficial for the improvement of creep resistance of Mg-Sn alloys.

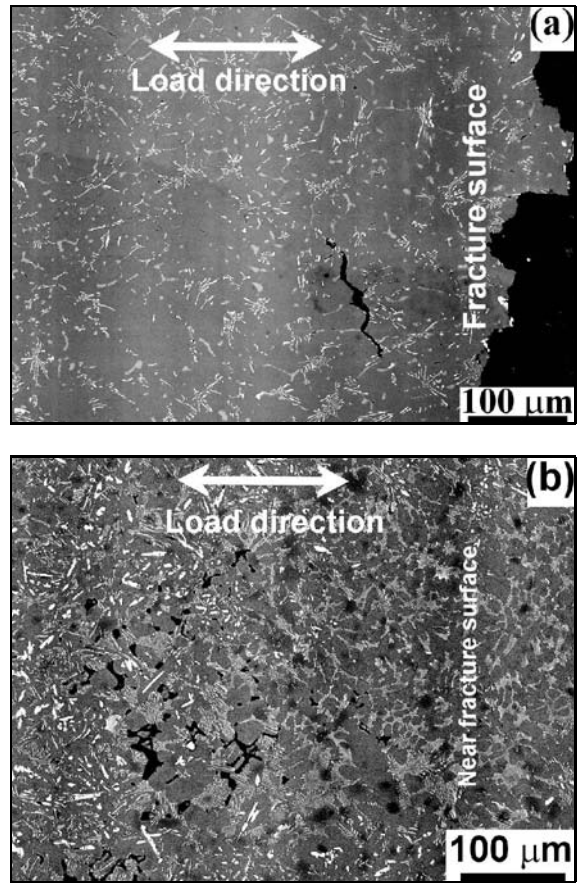

Fig. 12. Microstructures after tensile creep rupture: (a) Mg-3Sn-2Ca and (b) Mg-5Sn-2Ca.

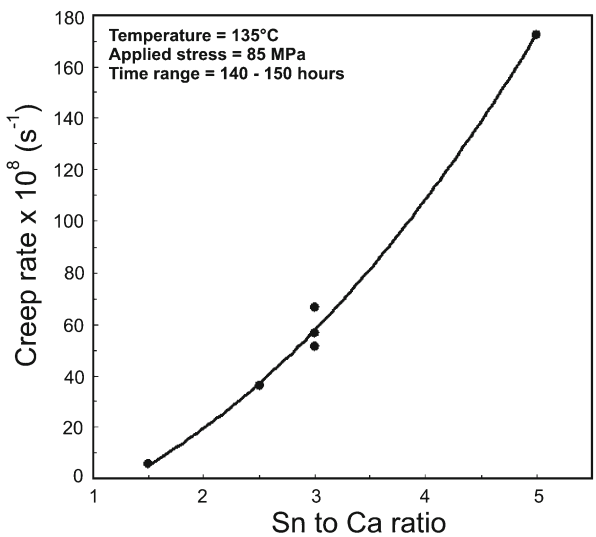

Fig. 13. Influence of the proportion of Sn to Ca on the measured creep rates of the selected alloys in the time range of 140–150 h.

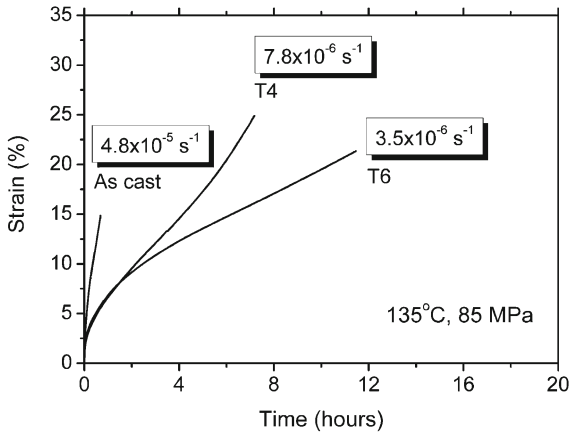

Fig. 14. Creep curves for the Mg-3Sn alloys with different states.

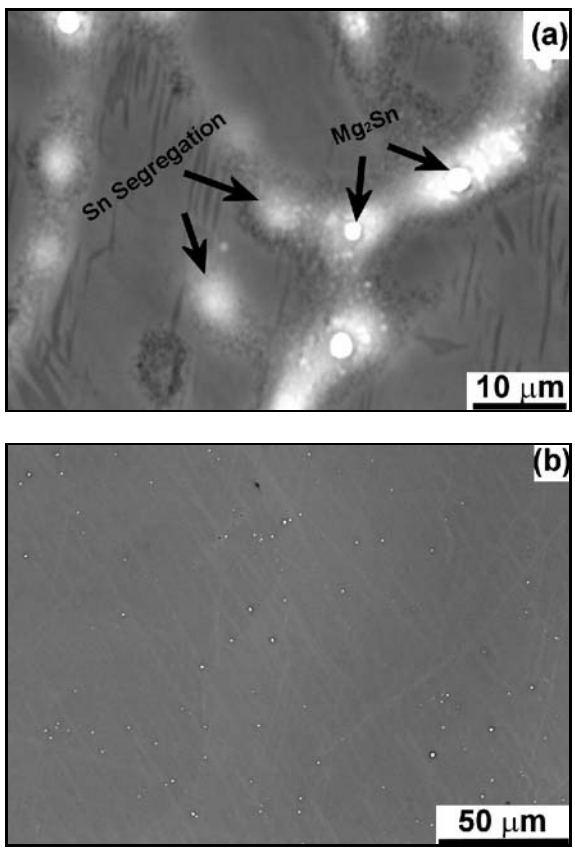

Fig. 15. Microstructure of the Mg-3Sn alloys without creep: (a) as-cast and (b) T4 heat treatment, 500 °C for 6 h.

3.2.3. Effect of the ratio of Sn to Ca

Figure 13 shows the creep rate as a function of Sn to Ca ratio. With the reduction of the ratio of Sn to Ca, the creep resistance improves. That means, if increasing the content of Ca and decreasing the content of Sn, the creep properties of Mg-Sn-Ca increase. This is in agreement with the above conclusions. If the content of Ca increases, the amount of CaMgSn and Mg_2Ca increases, the segregation of Sn reduces, both of these two factors lead to the improvement of creep properties. If the content of Sn increases, it can be expected that the Sn segregation becomes heavy and correspondingly the creep resistance is deteriorated. It is clearly evident from this figure that the relative ratio of Sn and Ca plays a very critical role in determining the creep resistance of Mg-Sn-Ca alloys rather than their individual amounts.

3.2.4. Effect of heat treatment

The compressive creep curves obtained at 135 °C and 85 MPa for the Mg-3Sn alloy in its as-cast state and after T4 and T6 heat treatments have been shown in Fig. 14. The as-cast Mg-3Sn alloy exhibits relatively lower creep resistance than the ones after T4 and T6 heat treatments. From the results it can be seen that the as-cast samples had a life of only 0.7 h with a high creep rate of $4.8 \times 10^{-5}\,s^{-1}$. On the other hand, the T4 heat treated sample had a life of 7.2 h (more than 10 times compared to that of as-cast) with a creep rate of $7.8 \times 10^{-6}\,s^{-1}$. After T6 heat treatment, the sample had a life of 11.4 hours with a creep rate of $3.5 \times 10^{-6}\,s^{-1}$.

In the T4 heat treated sample, unlike in the as-cast sample, the diffusive bright bands could not be observed (Fig. 15). The segregation of Sn is largely alleviated by this diffusion annealing treatment. After T6 heat treatment, fine particles Mg_2Sn were homogeneously precipitated in the magnesium matrix. Figure 16 shows the microstructure after creep for the Mg-3Sn alloys with different states. Voids can be observed at the dendritic boundaries. The cracks propagate along the dendritic boundaries, indicating that the deformation by boundary sliding plays an important role during the creep of these alloys. After creep, the fine particles Mg_2Sn were precipitated in the sample with T4 heat treatment (Fig. 16c). Their distribution is inhomogeneous. For the samples with T6 heat treatment, the distribution and amount of the second phase Mg_2Sn have no change after creep.

After T4 heat treatment, the segregation of Sn was alleviated and correspondingly the homologous temperature decreased. In addition, the fine particles Mg_2Sn were formed during creep which may be useful to hinder sliding of the grain boundaries and movement of the dislocations. Therefore, the creep resistance is improved after T4 heat treatment. In the sample with T6 heat treatment, more fine particles Mg_2Sn with better distribution are formed compared with the sample with T4 heat treatment. T6 heat treatment not only alleviates the segregation but also leads to the formation of hard second phases. As a

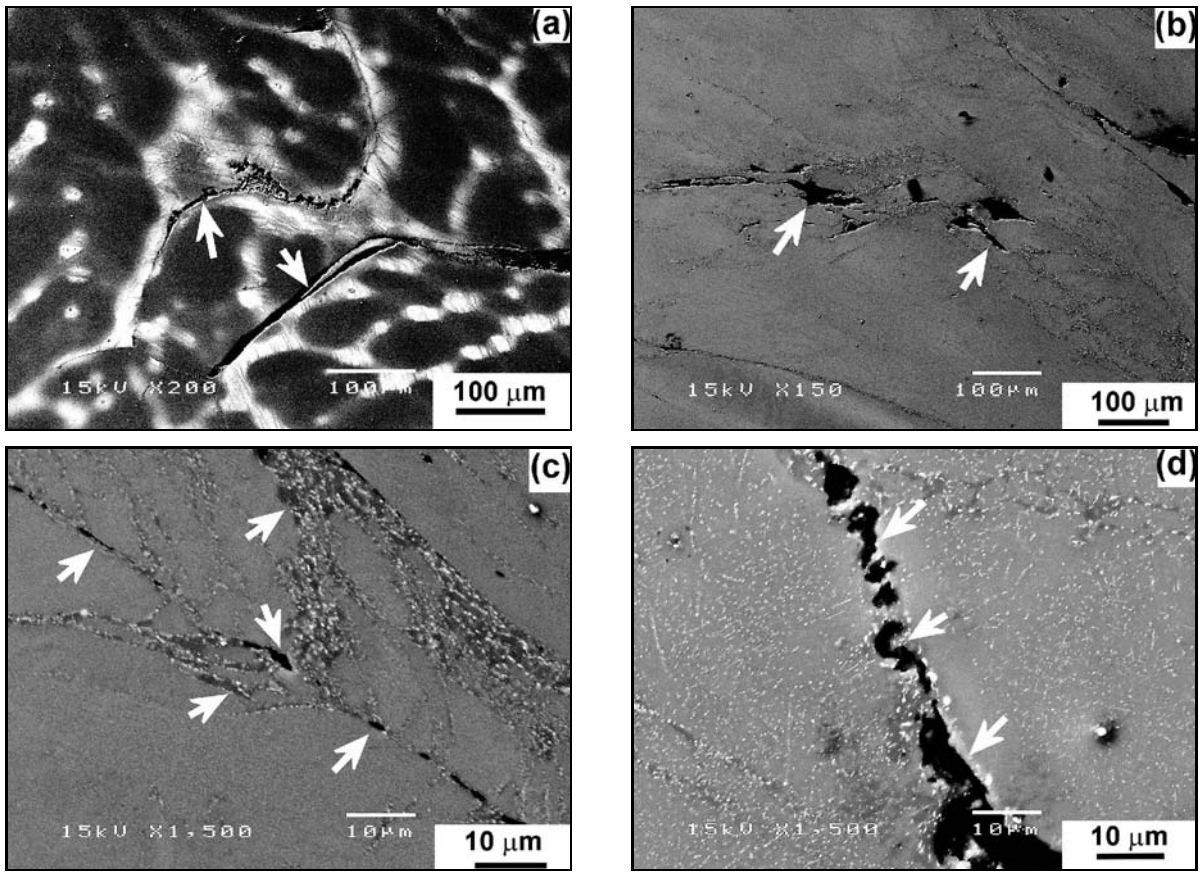

Fig. 16. Microstructure of the Mg-3Sn alloy after compressive creep at 135 °C and 85 MPa: (a) as-cast, (b) T4, at a low magnification, (c) T4, at large magnification and (d) T6. The cracks are marked by arrows.

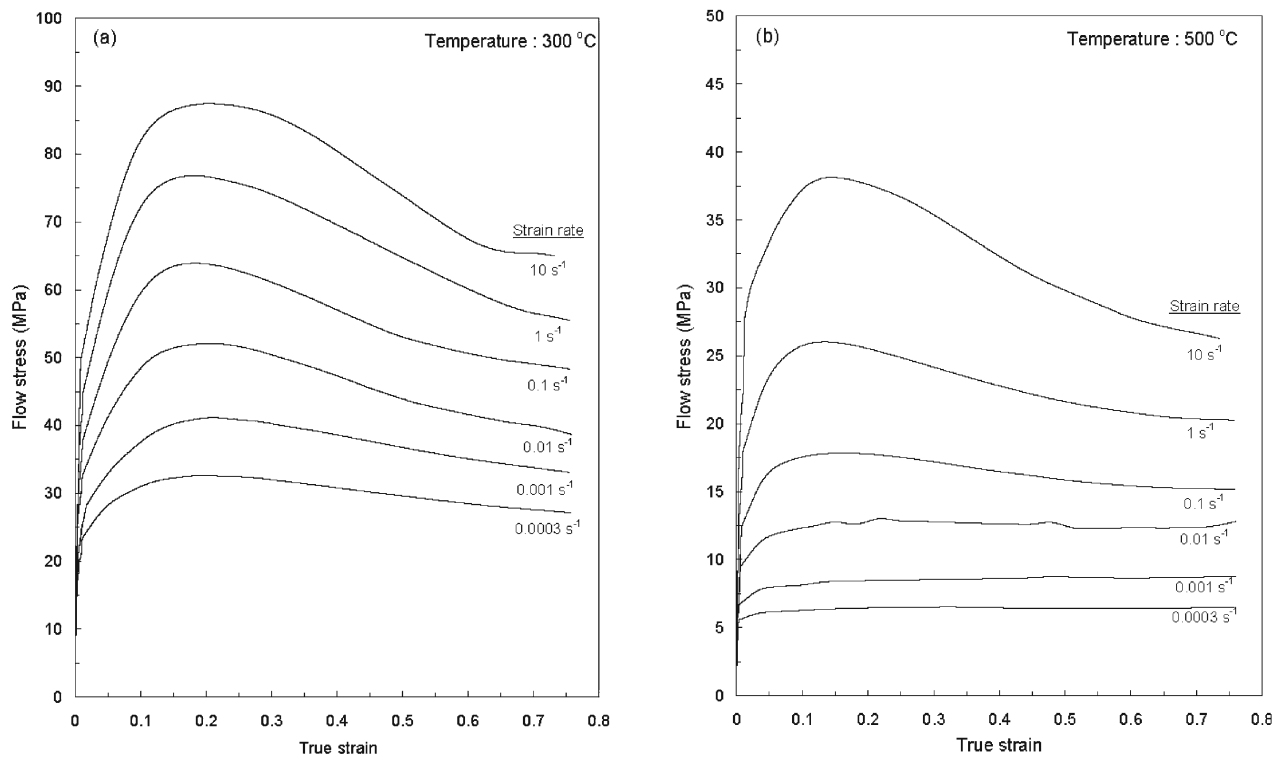

Fig. 17. Flow curves obtained on cast and homogenized Mg-3Sn-1Ca alloy deformed in compression at a temperature of (a) 300 °C and (b) 500 °C at different strain rates.

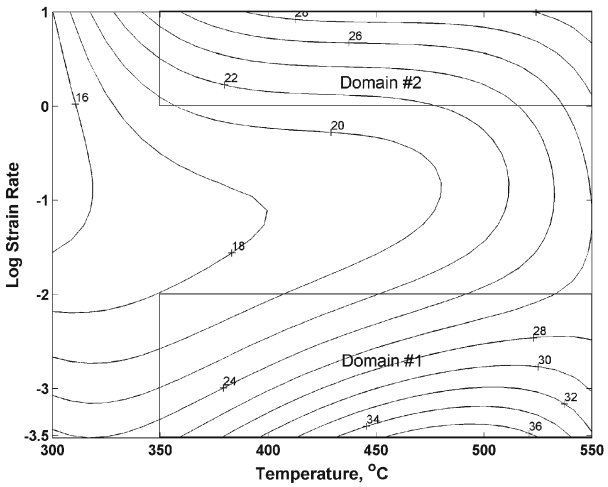

Fig. 18. Processing map obtained on cast and homogenized Mg-3Sn-1Ca alloy at a strain of 0.5. The numbers marked against the contours represent efficiency of power dissipation in percent.

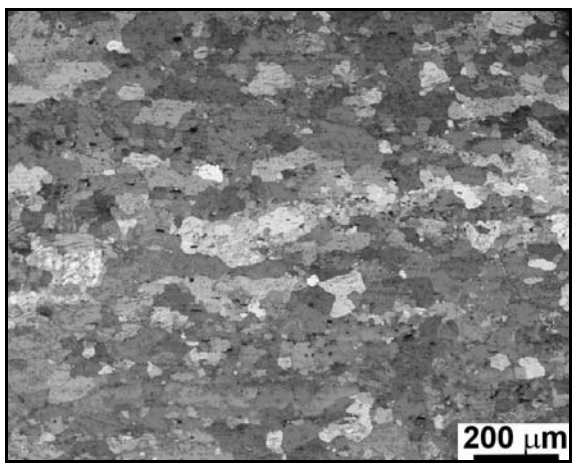

Fig. 19. Microstructure obtained on cast and homogenized Mg-3Sn-1Ca alloy. Extruded at 500 ℃ and an average strain rate of $3\,s^{-1}$.

result, the creep resistance can further be improved.

3.3. Hot deformation

The flow stress-true strain curves obtained on specimens deformed at temperatures 300 ℃ and 500 ℃ and at different strain rates are shown in Fig. 17. It reveals that the flow stress increased rapidly before softening occurred and flow softening is significant at lower temperatures and higher strain rates. The curves tend to exhibit steady-state flow at lower strain rates and higher temperatures.

The processing map at a strain of 0.5 is shown in Fig. 18. This strain may be considered large enough to represent steady-state flow. The map exhibits two domains, both occurring in the temperature range of 350–550 ℃. The first domain occurs in the lower strain rate range ($0.0003–0.01\,s^{-1}$) with a peak efficiency of about 36 % occurring at 500 ℃ and $0.0003\,s^{-1}$. The second domain occurs at higher strain rates in the range $1–10\,s^{-1}$ with a peak efficiency of 30 % occurring at 550 ℃ and $10\,s^{-1}$. The change-over occurs at a strain rate of about $0.1\,s^{-1}$. With a view to examine whether DRX (dynamic recrystallization) has occurred in the material during hot deformation, the material has been extruded at 500 ℃ and at a speed that is equivalent to an average strain rate of about $3\,s^{-1}$. The extrusion resulted in a sound product the microstructure of which is given in Figure 19, which shows that DRX has occurred at this temperature. The map did not exhibit any flow instability regime that could restrict the hot workability window.

In magnesium materials, four different slip systems operate if their critical resolved shear stress (CRSS) is exceeded and these are: (1) basal slip $\{0002\}\langle 11\bar{2}0\rangle$, (2) prismatic slip $\{10\bar{1}0\}\langle 11\bar{2}0\rangle$, (3) first order pyramidal slip $\{10\bar{1}1\}\langle 11\bar{2}0\rangle$ and $\{10\bar{1}2\}\langle 11\bar{2}0\rangle$, and (4) second order pyramidal slip $\{11\bar{2}2\}\langle 11\bar{2}3\rangle$. The basal slip has the lowest CRSS and is the easy slip system. In polycrystalline magnesium, prismatic slip contributes significantly to plastic flow at temperatures higher than about 225 ℃ and pyramidal slip beyond about 350 ℃. Thus, at temperatures higher than 350 ℃, steady state deformation has a large contribution from the pyramidal slip systems. Also, the simultaneous occurrence of dynamic restoration processes like DRX helps to soften the material and the recovery mechanisms leading to DRX are likely to be strain rate dependent – lattice self-diffusion at lower strain rates and grain boundary diffusion as a "short-circuit" mechanism at higher strain rates. Thus, two different DRX domains appear in the processing map – one at lower strain rates and the other at higher strain rates.

3.4. Corrosion

The corrosion rates measured using potentio-dynamic polarization and salt spray tests for a number of ternary Mg-Sn-Ca alloys are given in Table 5. Also included in the table are the results obtained on two binary Mg-Sn alloys for comparison. Several of the selected ternary alloys have shown higher corrosion resistance, i.e. lower corrosion rates, that are comparable with those measured for the binary magnesium alloys with tin. Though there are differences in the results obtained using the two different test methods, the trends are very similar. In general, salt spray test indicated higher corrosion rates for all the alloys.

To bring out the effect of individual alloying elements on corrosion rates, it is meaningful to change one alloying element at a time by keeping the other element constant. Such plots are given in Figs. 20 and

Table 5. Corrosion rates of different alloys with different proportions of Sn and Ca measured through potentio-dynamic polarization and salt spray tests

Alloy	Ratio of Sn : Ca	Corrosion rate (mm year^{-1})	
		Polarization test	Salt spray test
Mg-3Sn	NA	2.03	7.58
Mg-3Sn-1Ca	3 : 1	1.94	5.84
Mg-3Sn-1.5Ca	2 : 1	3.57	11.83
Mg-3Sn-2Ca	1.5 : 1	7.16	12.35
Mg-4.5Sn-1.5Ca	3 : 1	3.31	3.43
Mg-5Sn	NA	1.40	10.99
Mg-5Sn-1Ca	5 : 1	3.50	5.00
Mg-5Sn-1.5Ca	3.33 : 1	6.72	9.60
Mg-5Sn-2Ca	2.5 : 1	6.76	9.84
Mg-6Sn-2Ca	3 : 1	3.15	3.94

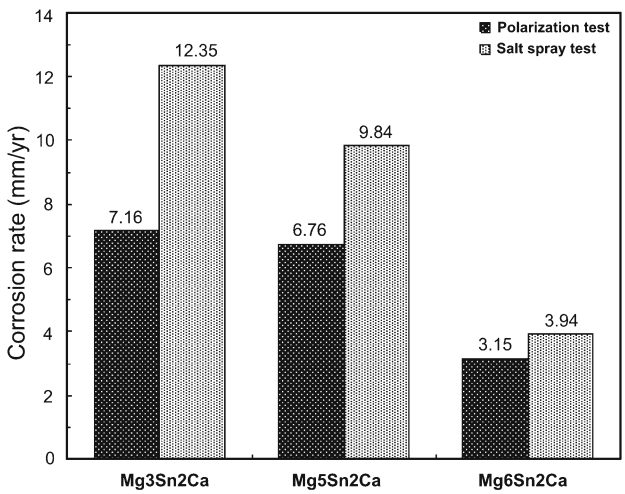

Fig. 20. Influence of the amount of Sn on the measured corrosion rates.

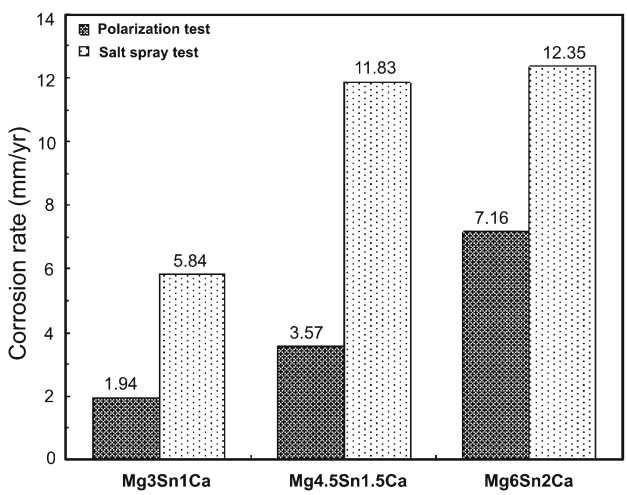

Fig. 21. Influence of the amount of Ca on the measured corrosion rates.

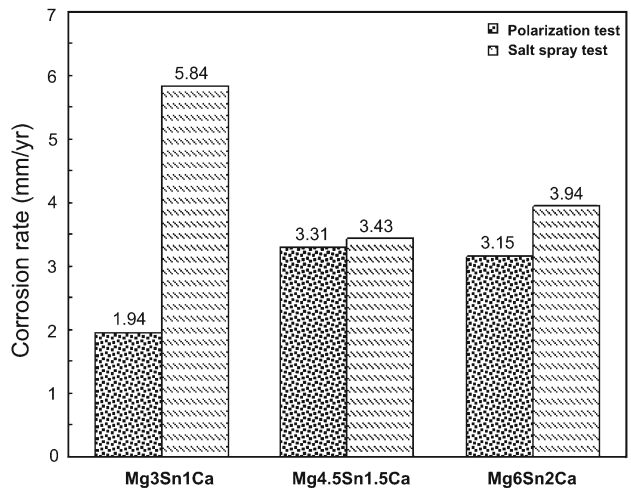

Fig. 22. Measured corrosion rates of alloys with same proportions of Sn and Ca.

21 for increasing amounts of tin and calcium, respectively. It is clear from Fig. 20 that increasing amount of tin improves the corrosion resistance in these alloys. This trend clearly indicates the beneficial role of tin in the ternary Mg-Sn-Ca alloys in reducing the corrosion of magnesium alloys, similar to that observed in the case of Mg-Sn binary alloys [5]. The results in Fig. 21 clearly indicate the detrimental role of calcium as far as corrosion resistance of these alloys is assessed. From these two figures it is now clear that tin and calcium have opposite effects as far as corrosion is concerned. However, from Fig. 20, one can also see that even with high calcium content (2 %) the ternary alloy Mg6Sn2Ca exhibited excellent corrosion resistance whereas the same amount of Ca in Mg3Sn2Ca gave poor corrosion resistance. Therefore, it may be more meaningful if the relative amounts of Sn and Ca are considered rather than amounts of individual elements. Figure 22 shows results obtained on three

alloys having the same ratio of Sn to Ca but with varying amounts of Sn and Ca. The figure indicates that the corrosion rates are similar for Mg4.5Sn1.5Ca and Mg6Sn2Ca alloys but not with Mg3Sn1Ca. The reason for this behaviour is yet unclear and needs further investigation. The ratio of Sn to Ca obviously plays a significant role in corrosion resistance of such ternary systems as well as the amount of alloying elements.

4. Conclusions

Sn is easy to segregate at the dendritic and grain boundaries. After the addition of Ca, the segregation of Sn can largely be alleviated. Only one second phase Mg_2Sn is identified in the binary Mg-Sn alloys. In the ternary Mg-Sn-Ca systems, Mg_2Sn and CaMgSn phases, or CaMgSn phase, or Mg_2Ca and CaMgSn phase can be observed which depends on the ratio of Sn to Ca. Among them, CaMgSn is very stable and cannot be dissolved even annealed at high temperatures for long time (T4 treatments).

During solidification, CaMgSn phase is first formed and then liquid magnesium starts solidifying. If the content of remaining Ca and Sn is over the critical value at the later stage of solidification, Mg_2Sn or Mg_2Ca are precipitated. The experimental results are in full agreement with that calculated by thermodynamic calculation.

The binary Mg-Sn alloys still have poor creep properties if Sn segregates at the dendritic and grain boundaries, which increases the homologous temperatures in these regions. After the addition of Ca, the creep resistance largely improves in the Mg-Sn-Ca alloys, because the second phases Mg_2Ca and CaMgSn act as obstacles to the sliding of boundaries during creep deformation. In addition, the harmful effects on the creep properties caused by Sn segregation are also alleviated by the addition of Ca.

The heat treatments affect the creep properties of binary Mg-Sn alloys. T4 and T6 treatments can improve the creep resistance, due to the alleviation of Sn segregation and/or the precipitation of fine Mg_2Sn.

The processing map exhibits two domains both in the temperature range 350–550 ℃ and one in the lower strain rate range ($0.0003–0.01\,s^{-1}$) and the other at higher strain rates ($1–10\,s^{-1}$). The microstructures of the alloy extruded at 500 ℃ at an average strain rate of about $3\,s^{-1}$ exhibited dynamically recrystallized microstructure.

The corrosion behaviour of these alloys from potentio-dynamic measurements and salt spray tests indicates that while Sn improves corrosion resistance of these alloys Ca has shown an opposite effect. However, an appropriate balance of Sn and Ca in the ratio of 3 to 1 is able to offer good corrosion resistance irrespective of their individual levels in the alloys studied.

The ratio of Sn to Ca plays a critical role in determining both the creep properties and corrosion resistance. It has a different effect on the creep properties and corrosion resistance. How to optimize the ratio of Sn to Ca is a key point to develop these alloys for powertrain applications.

Acknowledgements

The authors would like to thank Dr. Zisheng Zhen and Dr. Okechukwu Anopuo for their kind assistance during the preparation of this paper. The authors also highly acknowledge Prof. Schmid-Fetzer, Technische Universität Clausthal, for his very valuable thermodynamic calculations.

References

[1] EMLEY, E. F.: Principles of Magnesium Technology. Oxford, Pergamon 1966.
[2] AVEDESIAN, M. M.—BAKER, H.: ASM Specialty Handbook: Magnesium and Magnesium Alloys. Materials Park, OH, ASM International 1999.
[3] KAINER, K. U.: Magnesium Alloys and Technology. Weinheim, Germany, Wiley-VCH GmbH 2003. doi:10.1002/3527602046
[4] KAINER, K. U.—VON BUCH, F.: Materialwissenschaft und Werkstofftechnik, *30*, 1999, p. 159. doi:10.1002/(SICI)1521-4052(199903)30:3<159::AID-MAWE159>3.3.CO;2-W
[5] BOWLES, A. L.—DIERINGA, H.—BLAWERT, C.—HORT, N.—KAINER, K. U.: Materials Science Forum, *488–489*, 2005, p. 135. doi:10.4028/0-87849-968-7.135
[6] HORT, N.—HUANG, Y. D.—LEIL, T. A.—MAIER, P.—KAINER, K. U.: Advanced Engineering Materials, *8*, 2006, p. 359. doi:10.1002/adem.200600014
[7] ANOPUO, O.—HUANG, Y. D.—BLAWERT, C.—HORT, N.—KAINER, K. U.: In: Magnesium Technology 2006. Eds.: Luo, A., Neelameggham, N. R., Beals, R. S. San Antonio, Texas, TMS (The Minerals, Metals & Materials Society) 2006, p. 529.
[8] ABU LEIL, T.—RAO, K. P.—HORT, N.—KAINER, K. U.: In: Magnesium Technology 2006. Eds.: Luo, A. A., Neelameggham, N. R., Beals, R. S. San Antonio, Texas, TMS (The Minerals, Metals & Materials Society) 2006, p. 281.
[9] RAO, K. P.—PRASAD, Y. V. R. K.—HORT, N.—HUANG, Y. D.—KAINER, K. U.: Key Engineering Materials, *340–341*, 2007, p. 89. doi:10.4028/www.scientific.net/KEM.340-341.89
[10] ABU LEIL, T.—RAO, K. P.—HORT, N.—HUANG, Y. D.—BLAWERT, C.—DIERINGA, H.—KAINER, K. U.: In: Magnesium Technology 2007. Eds.: Beals, R. S., Luo, A., Neelameggham, N. R., Pekguleryuz, M. O. Orlando, Florida, TMS 2007, p. 257.
[11] KANG, D. H.—PARK, S. S.—KIM, N. J.: Materials Science and Engineering A, *413*, 2005, p. 555. doi:10.1016/j.msea.2005.09.022
[12] SASAKI, T.—OHISHI, K.—OHKUBO, T.—HONO, K.: Scripta Materialia, *55*, 2006, p. 251. doi:10.1016/j.scriptamat.2006.04.005

[13] MENDIS, C. L.—BETTLES, C. J.—GIBSON, M. A.—HUTCHINSON, C. R.: Materials Science and Engineering A, *435–436*, 2006, p. 163. doi:10.1016/j.msea.2006.07.090
[14] NAYEB-HASHEMI, A. A.—CLARK, J. B.: Phase Diagram of Binary Magnesium Alloys. Metal Park, OH, ASM International 1988.
[15] CHEN, D.—REN, Y.-P.—GUO, Y.—PEI, W.-L.—ZHAO, H.-D.—QIN, G.-W.: Transactions of Nonferrous Metals Society of China, *20*, 2010, p. 1321. doi:10.1016/S1003-6326(09)60298-3
[16] KIM, D. H.—LEE, J. Y.—LIM, H. K.—KYEONG, J. S.—KIM, W. T.: Materials Transactions, *49*, 2008, p. 2405. doi:10.2320/matertrans.MER2008140
[17] KIM, D. H.—LIM, H. K.—LEE, J. Y.—KIM, W. T.: Microstructural Evolution and Creep Resistance in Mg-Sn-Ca Alloy. In: Magnesium Technology 2008. Eds.: Pekguleryuz, M. O., Neelameggham, N. R., Beals, R. S., Nyberg, E. A. Warrendale, PA, TMS 2008, p. 417.
[18] KOZLOV, A.—OHNO, M.—ARROYAVE, R.—LIU, Z. K.—SCHMID-FETZER, R.: Intermetallics, *16*, 2008, p. 299.
[19] KOZLOV, A.—OHNO, M.—LEIL, T. A.—HORT, N.—KAINER, K. U.—SCHMID-FETZER, R.: Intermetallics, *16*, 2008, p. 316. doi:10.1016/j.intermet.2007.10.011
[20] LIU, H. M.—CHEN, Y. G.—TANG, Y. B.—WEI, S. H.—NIU, G.: Materials Science and Engineering: A, *464,* 2007, p. 124. doi:10.1016/j.msea.2007.02.061
[21] LIU, H. M.—CHEN, Y. G.—ZHAO, H. F.—WEI, S. H.—GAO, W.: Journal of Alloys and Compounds, *504*, 2010, p. 345. doi:10.1016/j.jallcom.2010.05.156
[22] NAYYERI, G.—MAHMUDI, R.: Materials Science and Engineering A, *527*, 2010, p. 669. doi:10.1016/j.msea.2009.08.056
[23] NAYYERI, G.—MAHMUDI, R.: Materials Science and Engineering A, *527*, 2010, p. 2087. doi:10.1016/j.msea.2009.11.053
[24] NAYYERI, G.—MAHMUDI, R.: Materials Science and Engineering A, *527*, 2010, p. 4613. doi:10.1016/j.msea.2010.04.015
[25] NAYYERI, G.—MAHMUDI, R.—SALEHI, F.: Materials Science and Engineering A, *527*, 2010, p. 5353. doi:10.1016/j.msea.2010.05.040
[26] PARK, K. C.—KIM, B. H.—JEON, J. J.—PARK, B. G.—PARK, Y. H.—PARK, I. M.: International Journal of Cast Metals Research, *21*, 2008, p. 96. doi:10.1179/136404608X361747
[27] PARK, K. C.—KIM, B. H.—KIMURA, H.—PARK, Y. H.—PARK, I. M.: Materials Transactions, *51*, 2010, p. 472. doi:10.2320/matertrans.M2009308
[28] SASAKI, T. T.—JU, J. D.—HONO, K.—SHIN, K. S.: Scripta Materialia, *61*, 2009, p. 80. doi:10.1016/j.scriptamat.2009.03.014
[29] WEI, S. H.—CHEN, Y. G.—TANG, Y. B.—ZHANG, X. P.—LIU, M.—XIAO, S. F.—ZHAO, Y. H.: Materials Science and Engineering A, *508*, 2009, p. 59. doi:10.1016/j.msea.2008.12.049
[30] YANG, M. B.—CHENG, L.—PAN, F. S.: Transactions of Nonferrous Metals Society of China, *20*, 2010, p. 584. doi:10.1016/S1003-6326(09)60182-5
[31] YANG, M. B.—MA, Y. L.—PAN, F. S.: Transactions of Nonferrous Metals Society of China, *19*, 2009, p. 1087. doi:10.1016/S1003-6326(08)60411-2
[32] YANG, M. B.—PAN, F. S.: Materials Science and Engineering A, *525*, 2009, p. 112. doi:10.1016/j.msea.2009.06.040
[33] YANG, M. B.—PAN, F. S.—CHENG, L.—SHEN, J.: Materials Science and Engineering A, *512*, 2009, p. 132. doi:10.1016/j.msea.2009.02.038
[34] ZHAO, H. D.—QIN, G. W.—REN, Y. P.—PEI, W. L.—GUO, Y.: Journal of Alloys and Compounds, *481*, 2009, p. 140. doi:10.1016/j.jallcom.2009.02.119
[35] HORT, N.—RAO, K. P.—ABU LEIL, T.—DIERINGA, H.—PRASAD, V.—KAINER, K. U.: Creep and Hot Working Behavior of a New Magnesium Alloy Mg-3Sn-2Ca. In: Magnesium Technology 2008. Eds.: Pekguleryuz, M. O., Neelameggham, N. R., Beals, R. S., Nyberg, E. A. Warrendale, PA, TMS 2008, p. 401.
[36] ZHAO, H. D.—QIN, G. W.—REN, Y. P.—PEI, W. L.—GUO, Y.: Journal of Alloys and Compounds, *481*, 2009, p. 140. doi:10.1016/j.jallcom.2009.02.119
[37] SCHMID-FETZER, R.—GROBNER, J.: Advanced Engineering Materials, *3*, 2001, p. 947. doi:10.1002/1527-2648(200112)3:12<947::AID-ADEM947>3.0.CO;2-P
[38] ABU LEIL, T.—RAO, K. P.—HORT, N.—DIERINGA, H.—BLAWERT, C.—HUANG, Y. D.—KAINER, K. U.: In: COM 2006: International Symposium on Magnesium Technology in the Global Age. Eds.: Pekguleryuz, M. O., Mackenzie, L. W. F. Montreal, The Metallurgical Society of CIM 2006, p. 739.
[39] HAN, Q. Y.—KAD, B. K.—VISWANATHAN, S.: Philosophical Magazine, *84*, 2004, p. 3843. doi:10.1080/14786430412331283073